The International Journal of Biochemistry & Cell Biology 45 (2013) 2420–2430

Contents lists available at ScienceDirect

The International Journal of Biochemistry & Cell Biology

journal homepage: www.elsevier.com/locate/biocel

Novel 2-(substituted benzyl)quinuclidines inhibit human α7 and α4β2 nicotinic receptors by different mechanisms

Hugo R. Arias [a,*], Jhon J. López [b], Dominik Feuerbach [c], Angélica Fierro [b], Marcelo O. Ortells [d], Edwin G. Pérez [b]

[a] Department of Medical Education, California Northstate University College of Medicine, Elk Grove, CA 95757, USA
[b] Facultad de Química, Pontificia Universidad Católica de Chile, Santiago 6094411, Chile
[c] Novartis Institutes for Biomedical Research, Basel, Switzerland
[d] Faculty of Medicine, University of Morón – CONICET, Argentina

ARTICLE INFO

Article history:
Received 18 April 2013
Received in revised form 11 July 2013
Accepted 6 August 2013
Available online 14 August 2013

Keywords:
Quinuclidines
Nicotinic acetylcholine receptors
Competitive antagonists
Noncompetitive antagonists
Structure–activity relationship

ABSTRACT

This work presents the design and synthesis of a series of novel 2-benzylquinuclidine derivatives, comprising 12 methiodide and 11 hydrochloride salts, and their structural and pharmacological characterization at the human (h) α7 and α4β2 nicotinic receptors (nAChRs). The antagonistic potency of these compounds was tested by Ca^{2+} influx assays on cells expressing the hα7 or hα4β2 nAChR subtype. To determine the inhibitory mechanisms, additional radioligand binding experiments were performed. The results indicate that the methiodides present the highest affinities for the hα7 nAChR agonist sites, while the same compounds bind preferably to the hα4β2 nAChR ion channel domain. These results indicate that the methiodides are competitive antagonists of the hα7 nAChR but noncompetitive antagonists of the hα4β2 subtype. Docking and molecular dynamics simulations showed that the methiodide derivative **8d** binds to the hα7 orthosteric binding sites by forming stable cation-π interactions between the quaternized quinulinuim moiety and the aromatic box in the receptor, whereas compounds **7j** and **8j** block the hα4β2 AChR ion channel by interacting with a luminal domain formed between the serine (position 6′) and valine (position 13′) rings that overlaps the imipramine binding site.

1. Introduction

The homomeric receptor α7 and the heteromeric receptor α4β2 are the most prominent nicotinic acetylcholine receptors (nAChRs) in the brain. These pentameric nAChRs present five (i.e., α7 nAChRs) and two (i.e., α4β2 nAChRs) agonist binding sites located at the interface of the α7/α7 and α4/β2 subunits, respectively. The structures of the *Torpedo* AChR at 4 Å resolution (Unwin, 2005) and of the acetylcholine binding proteins (AChBPs) (e.g., see Celie et al., 2004) have been used for many years as models for the whole nAChR and for the extracellular domain containing the agonist binding sites, respectively, as well as models for the entire Cys-loop ligand-gated receptor superfamily, including $GABA_A$ and $GABA_B$, type 3 serotonin, and glycine receptors (reviewed in Arias, 2006; Arias et al., 2006; Albuquerque et al., 2009).

Although nAChRs in general are expressed in neuronal cells (reviewed in Arias, 2006; Arias et al., 2006; Albuquerque et al., 2009), α7 nAChRs are also expressed in non-neuronal cells (reviewed in Romanelli et al., 2007; Mousa and Arias, 2010). Consequently, α7 and α4β2 nAChRs are implicated in diseases such as drug addiction, depression, neuronal and peripheral inflammation, and cancer, whereas α7 AChRs are also important components in the development of Alzheimer's disease and schizophrenia (reviewed in Albuquerque et al., 2009; Romanelli et al., 2007; Mousa and Arias, 2010; Tuppo and Arias, 2005). Several laboratories have developed agonists with selectivity for the α4β2 or α7 nAChR subtype (Arias et al., 2010a; Feuerbach et al., 2007; reviewed in Mazurov et al., 2006; Hurst et al., 2013). Excellent examples of selective agonists are varenicline, a partial agonist of the α4β2 nAChR that is currently used for the treatment of nicotine addiction, and TC-5619, an α7 nAChR agonist that is in clinical phase 2 for the treatment of cognitive deficits (reviewed in Hurst et al., 2013). In addition, the interest in nAChRs antagonists has increased lately because of their possible pharmacological use as antidepressants, anti-addictive, anti-psychotic, and neuroprotective agents, as potential therapy for organophosphorus nerve agent intoxication,

Abbreviations: nAChR, nicotinic acetylcholine receptor; ACh, acetylcholine; CCh, carbamylcholine; [^{3}H]MLA, [^{3}H]methyllycaconitine; RT, room temperature; IC_{50}, ligand concentration that produces 50% inhibition (of binding or of agonist activation); K_i, inhibition constant; n_H, Hill coefficient; EC_{50}, agonist concentration that produces 50% AChR activation; RMSD, root mean square deviation.

* Corresponding author. Tel.: +1 19166470458; fax: +1 19166867310.
E-mail address: hugo.arias@cnucom.org (H.R. Arias).

1357-2725/$ – see front matter © 2013 Elsevier Ltd. All rights reserved.
http://dx.doi.org/10.1016/j.biocel.2013.08.003

and because their anti-proliferation, anti-migration, and antiangiogenic activities suitable for cancer treatment (Ferchmin et al., 2013; Sadek et al., 2012; Paleari et al., 2009; Sheridan et al., 2005; Pérez et al., 2013). Among them, we can include the selective α7 nAChR antagonists, N3,N7-diaminophenothiazinium derivatives (Sadek et al., 2012) and 1-(1-benzyl-1*H*-indol-3-yl)-*N*,*N*,*N*-trimethylmethanaminium iodides (Pérez et al., 2013), and the selective α4β2 nAChR antagonists, diazaspirocyclic compounds (Strachan et al., 2012). Thus, an improved understanding of the functional and structural interaction of selective α7 or α4β2 nAChR antagonists is crucial to the development of safer ligands for different therapeutic uses.

The nicotinoid pharmacophore spans two important moieties which determine both selectivity and potency: a center containing a positively charged nitrogen group that interacts with the well-characterized "aromatic box" of the nAChR; and a nitrogen-containing heterocycle that form a hydrogen bond with the complementary subunit in the receptor and is important for agonist activity (Blum et al., 2010). The work by Crooks et al. (1995) has led to the discovery of several nAChR antagonists which potently inhibit selective nAChR subtypes. They showed that *N*-n-alkylation of the pyridine nitrogen atom of nicotine with C1–C12 carbon chains converted nicotine from a potent agonist into potent and subtype-selective nAChR antagonists. This suggests that compounds with a center containing a positively charged nitrogen group that interacts with the well-characterized "aromatic box" of the nAChR linked with a non-pyridinic aromatic ring should act as nAChR antagonists. Additionally, the bicycle quinuclidine (1-azabicycle[2.2.2]octane) is frequently mentioned in the design and synthesis of potent and selective ligands for the α7 nAChR subtype (Mazurov et al., 2006). Using this approach and looking for potent and selective antagonists for the α7 nAChR subtype, a new series of 2-(substituted benzyl)quinuclidines were designed and their chemical identities characterized. Subsequently, the pharmacological activity of each antagonist was determined by Ca^{2+} influx experiments on cell lines expressing human (h) α7 or hα4β2 nAChRs, and the mechanisms of inhibition were differentiated by radioligand binding assays. Finally, the binding site locations and the structural components of these sites were characterized on each receptor subtype by molecular docking and molecular dynamics studies.

2. Material and methods

2.1. Material

[^{3}H]Imipramine (47.5 Ci/mmol) and [^{3}H]cytisine (35.6 Ci/mmol) were obtained from PerkinElmer Life Sciences Products, Inc. (Boston, MA, USA), and [^{3}H]methyllycaconitine ([^{3}H]MLA) (100 Ci/mmol) was purchased from American Radiolabeled Chemicals Inc. (St. Louis, MO, USA). Imipramine hydrochloride and carbamylcholine dichloride (CCh) were purchased from Sigma Chemical Co. (St. Louis, MO, USA). (±)-Epibatidine hydrochloride was obtained from Tocris Bioscience (Ellisville, MO, USA). κ-Bungarotoxin (κ-BTx) was obtained from Biotoxins Inc. (St. Cloud, FL, USA).

2.2. Methods

2.2.1. Chemical synthesis

A new series of 2-(substituted benzyl)quinuclidines and *N*-methyl-2-(substituted benzyl)quinuclidinium iodides were synthesized as follow: (i) the hydroxyl benzaldehydes (**1**–**4**) were converted into the corresponding alkyloxy benzaldehydes (**5a**–**5k**) by the classical Williamson methodology using K_2CO_3 and ethanol as base and solvent respectively; (ii) the alkyloxy aldehydes were coupled with 3-quinuclidinone in a basic media to furnish the corresponding (Z)-2-benzylidenequinuclidin-3-ones (**6a**–**6k**); (iii) these α,β-unsaturated carbonyl compounds were completely reduced in two steps using H_2, Pd/C and the Wolff-Kishner reaction to produce the 2-(substituted benzyl)quinuclidines (**7a**–**7k**); and finally, (iv) the quinuclidines were quaternized with methyl iodide in acetone to obtain the *N*-methyl-2-(substituted benzyl)quinuclidinium iodides (**8a**–**8k**).

2.2.2. Chemical characterization

Melting points were determined on a Reichert Galen III hot plate microscope apparatus and are uncorrected. ^{1}H NMR spectra were recorded on Bruker ACP-200 or Bruker Avance 400 at 200 or 400 MHz, respectively. ^{13}C NMR spectra were recorded on the same instruments at 50 or 100 MHz. The results are detailed in Supplemental Information. Chemical shifts are reported in δ values (parts per million, ppm) relative to an internal standard of tetramethylsilane in $CDCl_3$ or DMSO-d_6 and coupling constants (J) are given in Hertz. Precoated silica gel 60 plates (Merck 60 F_{254} 0.2 mm) were used for TLC. TLC spots were visualized by spraying with Dragendorff's reagent or by UV light at 254 nm.

2.2.3. Ca^{2+} influx measurements in cells containing different AChR subtypes

Ca^{2+} influx assays were performed on HEK293-hα4β2 and GH3-hα7 cells using the procedures previously described (Arias et al., 2010a,b,c, 2011). Briefly, cells were seeded 48 h prior to the experiment on black 96-well plates (Costar, New York, USA) at a density of 5×10^4 per well and incubated at 37 °C in a humidified atmosphere (5% CO_2/95% air). The medium was changed to 1% FBS in HEPES-buffered salt solution (HBSS) (130 mM NaCl, 5.4 mM KCl, 2 mM $CaCl_2$, 0.8 mM $MgSO_4$, 0.9 mM NaH_2PO_4, 25 mM glucose, 20 mM HEPES, pH 7.4) 16–24 h before the experiment. On the day of the experiment, the medium was removed by flicking the plates and replaced with 100 μL HBSS/1% BSA containing 2 μM Fluo-4 (Molecular Probes, Eugene, OR, USA) in the presence of 2.5 mM probenecid (Sigma, Buchs, Switzerland). The cells were then incubated at 37 °C in a humidified atmosphere (5% CO_2/95% air) for 1 h. Plates were flicked to remove excess of Fluo-4, washed twice with HBSS, and then placed in the cell plate stage of the fluorimetric imaging plate reader (Molecular Devices, Sunnyvale, CA, USA). To measure the inhibitory activity of the compounds, each compound was added at the concentrations indicated in the figures instead of the second washing step, and pre-incubated for 5 min at RT. Thereafter, (±)-epibatidine (0.1 μM) was added from the agonist plate to the cell plate using the 96-tip pipettor, and the fluorescence was recorded for 3 min. For all measurements, a baseline consisting of 5 measurements of 0.4 s each was recorded. The laser excitation and emission wavelengths are 488 and 510 nm, at 1 W, and a CCD camera opening of 0.4 s.

The concentration–response data were curve-fitted, and the IC_{50} and Hill coefficient (n_H) values were calculated by nonlinear least squares analysis using the Prism software (GraphPad Software, San Diego, CA).

2.2.4. Radioligand competition binding experiments

Radioligand experiments were performed using membranes prepared from HEK293-hα4β2 and SHSY5Y-hα7 cells as described previously (Arias et al., 2010a,b,c, 2011). We first compared the effect of novel ligands on [^{3}H]cytisine binding to hα4β2 nAChRs and on [^{3}H]MLA binding to hα7 nAChRs, using the method previously developed in our laboratory (Arias et al., 2010a, 2011). To determine the interaction of these compounds with the nAChR ion channels, additional [^{3}H]imipramine competition binding experiments were performed as described previously

(Arias et al., 2010a,b). In this regard, nAChR membranes (1.5 mg/mL) were suspended in binding saline (BS) buffer (50 mM Tris–HCl, 120 mM NaCl, 5 mM KCl, 2 mM $CaCl_2$, 1 mM $MgCl_2$, pH 7.4) with 4.1 nM [^{3}H]MLA, 7.7 nM [^{3}H]cytisine, or 18 nM [^{3}H]imipramine, in the presence of 0.1 μM (±)-epibatidine (AChRs are mainly in the desensitized state), and preincubated for 20 min at room temperature (RT). The nonspecific binding was determined in the presence of 1 mM CCh ([^{3}H]cytisine), 1 μM (±)-epibatidine ([^{3}H]MLA), and 100 μM imipramine ([^{3}H]imipramine). The total volume was divided into aliquots, and increasing concentrations of the ligand under study was added to each tube and incubated for 90 min at RT. AChR-bound radioligand was then separated from free ligand by a filtration assay and the radioactivity was determined by scintillation counting as previously described (Arias et al., 2010a,b,c, 2011).

The IC_{50} and n_H values were calculated by nonlinear least squares analysis using the Prism software. The IC_{50} values were transformed into inhibition constant (K_i) values using the Cheng–Prusoff relationship (Cheng and Prusoff, 1973):

$$K_i = \frac{IC_{50}}{1 + ([[^3H]\text{ligand}]/K_d^{\text{ligand}})} \quad (1)$$

where [[^{3}H]ligand] is the initial concentration of [^{3}H]MLA, [^{3}H]cytisine, or [^{3}H]imipramine, and K_d^{ligand} is the dissociation constant for [^{3}H]MLA at the hα7 nAChR (1.86 nM; Davies et al., 1999), [^{3}H]cytisine at the hα4β2 nAChR (0.3 nM; Zhang and Steinbach, 2003), and for [^{3}H]imipramine at the hα4β2 nAChR (0.83 μM; Arias et al., 2010c) and hα7 (1 μM; Arias et al., 2010b) AChRs, respectively. The K_i and n_H values were summarized in Table 4.

2.2.5. Homology modeling

To construct the extracellular domain of the hα7 and hα4β2 nAChRs, the structure of the AChBP from *Lymnaea stagnalis* (Ls-AChBP) in complex with nicotine at 2.2 Å resolution (PDB 1UW6) (Celie et al., 2004) was used as a template for homology modeling. The target protein and template were aligned using the Multalin server (Corpet, 1988). The *Torpedo* nAChR at a resolution of ~4 Å (PDB 2BG9) (Unwin, 2005) was used as a template for the construction of the hα7 and hα4β2 nAChR models, using the MODELLER9v6 (Šali and Blundell, 1993). In this study, 100 runs were carried out using standard parameters and the outcomes were ranked on the basis of the internal scoring function of the program. The best model was chosen as the target model.

2.2.6. Molecular docking

In order to obtain information about the most important nAChR–ligand interactions, molecular docking experiments were performed using AutoDock 4.0 (Morris et al., 1998) and AutoDock Vina (version 1.1.1) (Trott and Olson, 2010). The energy of binding of the best docked compounds was calculated by AutoDock 4.0, AutoDock Vina, and by molecular mechanics (i.e., difference between the energy of the ligand–receptor complex and the sum of energies of the isolated receptor and ligand).

For the docking to the orthosteric binding sites, the grid maps were calculated using the autogrid option and centered on the binding sites. The volumes chosen for the grid maps were made up of 60 × 60 × 60 points, with a grid-point spacing of 0.375 Å. For the transmembrane domains, a grid covering the whole region was used instead. The autotors option was used to define the rotating bonds in the ligand. In the Lamarckian genetic algorithm dockings, the number of individuals in a population of 1500, a maximum number of 2.5×10^6 energy evaluations, a maximum number of 27,000 generations, a mutation rate of 0.02, and a cross-over rate of 0.80, were employed. The protonated enantiomers of **8d**, **7j**, and **8j** docked to the respective nAChR were built using the lowest docked-energy binding positions using Gaussian03 (Frisch et al., 2004), and the partial charges were corrected using electrostatic potential methodology (Chipot et al., 1992; Ángyán, 1995).

2.2.7. Refinement of the complex by molecular dynamics simulations

Molecular dynamics (MD) simulations (5–10 ns) were carried out for (*R*)-**8d**, (*S*)-**7j**, and (*S*)-**8j** docked to the hα7 and hα4β2 nAChRs, respectively. The receptors were solvated and ions (i.e., 0.2 M NaCl) were added to create an overall neutral system using the program solvate 1.0 (Grubmueller, 1996). The final system was submitted to MD simulations using NAMD 2.6 (Phillips et al., 2005) and the CHARMM force field. The isothermal–isobaric ensemble was used to perform MD calculations. Periodic boundary conditions were applied to the system in the three coordinate directions. Pressure of 1 atm and temperature of 300 or 310 K were maintained throughout the experiment. Particle mesh Ewald algorithm was applied to calculate electrostatic forces in our systems. Cutoffs of 12 Å and time step of 1 fs were used in all simulations. Model building and analysis were performed by using visual molecular dynamics (VMD) (Humphrey et al., 1996).

The stability of the cation-π interaction observed for the ligand in each orthosteric binding site was evaluated by following the distance between C-6 from hα7-Trp171 (or hα4-Trp182) and N from the ammonium group of (*R*)-**8d** during 5-ns. For this purpose, the procedure defined in distance.tcl (which calculates the distance between two atom selections) into the VMD was used.

The root mean square deviation (RMSD) values were calculated as described in Supplementary Information. To give an estimation of the stability of the ligand conformers within the luminal site, the RMSD variance during the last 3 ns of simulation was also calculated. The lower the RMSD variance, the more stable the conformer is.

3. Results

3.1. Chemical synthesis

A series of novel 2-(substituted benzyl)quinuclidine (**7**) and *N*-methyl-2-(substituted benzyl)quinuclidinium iodides (**8**) (see structures in Table 1) were synthesized according to Scheme 1. The Williamson method was initially used to couple hydroxyl benzaldehydes (**1**–**4**) and alkyl bromides to produce the corresponding alkyloxy benzaldehydes (**5a**–**k**). The **5a**–**k** compounds were subsequently coupled with 3-quinuclidinone, producing the α,β-unsaturated ketones (**6a**–**k**) (Vijayakumar et al., 2003, 2005). The C—C double bond was hydrogenated using palladium/charcoal as catalyst, and a modified Wolff-Kishner strategy (Scheiber and Nemes, 2008) was used to reduce the carbonyl group to furnish the desired compounds (**7a**–**7k**). The corresponding methylammonium iodides (**8a**–**k**) were obtained by adding methyl iodide to the tertiary amines **7**. Finally, compound **9** is an intermediate in the synthesis of **7c** and **8c** which was quaternized as mentioned above.

3.2. Structure–activity relationships studies using Ca^{2+} influx assays

Fig. 1 shows that (±)-epibatidine-induced Ca^{2+} influx in HEK293-hα4β2 and GH3-hα7 cells is inhibited by pre-incubation with compounds **7b**–**k**, **8b**–**k**, and **9**. The compounds showed IC_{50} values in the micromolar or submicromolar range for the hα4β2 and hα7 nAChRs (Table 2). The only exceptions were **7a** which was inactive at both subtypes, and **8a** that was barely active at the hα4β2 nAChR (IC_{50} > 100 μM; Table 2) compared to the hα7 nAChR. These functional results permitted to analyze the structure–activity relationships of these compounds based on the substitution pattern

Table 1
Molecular structures of compounds **7a**–**k**, **8a**–**k**, and **9**.

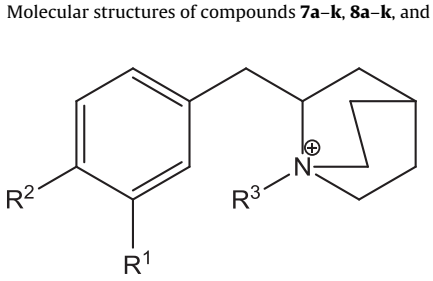

7-8

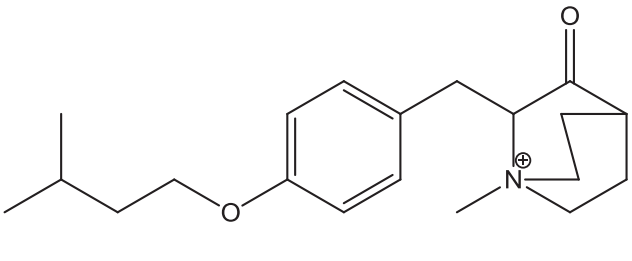

9

Compound	R^1	R^2	R^3
7a	H	OCH_3	H
7b	H	$O(CH_2)_2CH_3$	H
7c	H	$O(CH_2)_2CH(CH_3)_2$	H
7d	H	$O(CH_2)_5CH_3$	H
7e	H	$O(CH_2)_7CH_3$	H
7f	$O(CH_2)_2CH(CH_3)_2$	H	H
7g	$O(CH_2)_5CH_3$	H	H
7h	OCH_3	$O(CH_2)_2CH(CH_3)_2$	H
7i	OCH_3	$O(CH_2)_5CH_3$	H
7j	$O(CH_2)_2CH(CH_3)_2$	OCH_3	H
7k	$O(CH_2)_5CH_3$	OCH_3	H
8a	H	OCH_3	CH_3
8b	H	$O(CH_2)_2CH_3$	CH_3
8c	H	$O(CH_2)_2CH(CH_3)_2$	CH_3
8d	H	$O(CH_2)_5CH_3$	CH_3
8e	H	$O(CH_2)_7CH_3$	CH_3
8f	$O(CH_2)_2CH(CH_3)_2$	H	CH_3
8g	$O(CH_2)_5CH_3$	H	CH_3
8h	OCH_3	$O(CH_2)_2CH(CH_3)_2$	CH_3
8i	OCH_3	$O(CH_2)_5CH_3$	CH_3
8j	$O(CH_2)_2CH(CH_3)_2$	OCH_3	CH_3
8k	$O(CH_2)_5CH_3$	OCH_3	CH_3

on the benzene ring, including the length of the alkyloxy group (C_1 to C_8), the presence of a hydroxyl group, and the effect of a carbonyl group on the quinuclidine ring system.

(1) In general, N-methylquinolidinium iodides (**8a**–**8k**) showed stronger antagonistic activities than their quinolinium chloride (**7b**–**7k**) counterparts, and this effect is more marked for the hα7 subtype.

(2) The *para* substitution with a long chain increases the selectivity for the hα7 nAChR (**8a-e**). A hexyloxy group (**8d**) at this position is close to the optimal selectivity for the hα7 nAChR because both shorter [e.g., methyloxy (**8a**), propyloxy (**8b**),

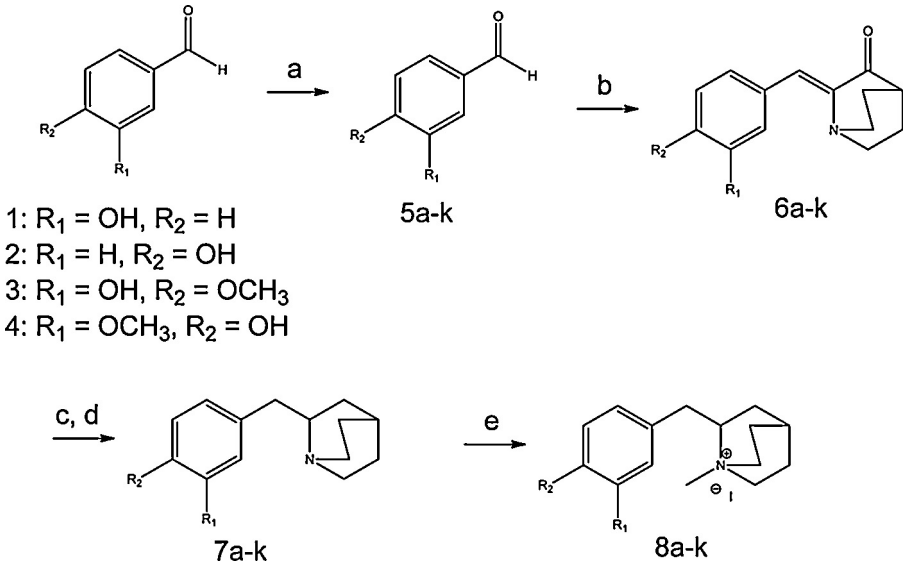

Scheme 1. Experimental conditions. (a) K_2CO_3, R-X, EtOH, reflux, 18 h. (b) KOH, MeOH, reflux, 24 h. (c) H_2, Pd/C, MeOH. (d) H_2N–NH_2, KOH, diglyme, 180 °C, 24 h. (e) CH_3I, acetone, RT, 16 h. In this sequence the hydroxybenzaldehydes (**1**–**4**) are converted to alkoxybenzaldehydes (**5a**–**k**), which are coupled with 3-quinuclidinone to form the α,β-unsaturated ketones (**6a**–**k**). This is followed by catalytic hydrogenation and carbonyl group reduction to furnish the 2-benzylquinuclidines (**7a**–**k**). Quaternization with methyl iodide produces the methyl quinolinium salts (**8a**–**k**).

Table 2
Inhibitory potency of the studied compounds on the hα4β2 and hα7 nAChRs determined by Ca^{2+} influx experiments.

Compound	hα4β2		hα7		hα7/hα4β2
	IC_{50} (μM)	n_H	IC_{50} (μM)	n_H	
7a	>100	–	>100	–	–
7b	4.9 ± 1.1	1.19 ± 0.04	6.7 ± 2.9	1.78 ± 0.30	1.4
7c	1.2 ± 0.5	1.40 ± 0.43	2.2 ± 0.1	1.64 ± 0.54	1.8
7d	1.1 ± 0.2	1.25 ± 0.18	2.1 ± 0.1	2.42 ± 0.20	1.9
7e	3.8 ± 0.1	1.14 ± 0.24	3.8 ± 0.2	2.06 ± 0.54	1.0
7f	0.8 ± 0.1	1.34 ± 0.41	3.7 ± 0.3	1.76 ± 0.11	4.5
7g	1.0 ± 0.1	1.50 ± 0.17	3.6 ± 0.1	1.97 ± 0.12	3.6
7h	1.3 ± 0.2	0.99 ± 0.04	4.0 ± 1.0	1.99 ± 0.49	3.2
7i	2.0 ± 0.8	1.38 ± 0.05	3.3 ± 0.4	2.04 ± 0.35	1.6
7j	1.3 ± 0.4	0.98 ± 0.30	13.0 ± 1.7	1.42 ± 0.06	9.8
7k	0.6 ± 0.1	1.14 ± 0.05	2.5 ± 0.2	1.62 ± 0.09	4.0
8a	>100	–	12.5 ± 1.0	2.19 ± 0.34	–
8b	15.2 ± 5.1	0.97 ± 0.17	3.6 ± 0.1	2.34 ± 0.18	0.2
8c	0.4 ± 0.1	0.89 ± 0.09	1.2 ± 0.1	1.99 ± 0.37	3.3
8d	2.5 ± 0.1	1.44 ± 0.27	0.5 ± 0.1	2.26 ± 0.02	0.2
8e	0.9 ± 0.1	1.04 ± 0.01	0.8 ± 0.1	2.08 ± 0.38	0.8
8f	0.9 ± 0.2	1.02 ± 0.13	3.7 ± 0.8	1.87 ± 0.20	4.2
8g	2.4 ± 0.1	1.09 ± 0.07	0.9 ± 0.1	2.06 ± 0.42	0.4
8h	1.8 ± 0.2	1.21 ± 0.25	3.5 ± 0.2	2.18 ± 0.18	1.9
8i	0.4 ± 0.1	1.20 ± 0.19	1.1 ± 0.1	2.02 ± 0.39	3.2
8j	1.7 ± 0.4	0.76 ± 0.05	18.0 ± 2.6	1.98 ± 0.14	10.4
8k	1.0 ± 0.3	0.98 ± 0.04	2.9 ± 0.9	2.29 ± 0.24	2.9
9	3.6 ± 0.7	1.10 ± 0.10	12.0 ± 0.3	2.17 ± 0.10	3.4

The IC_{50} and n_H values were calculated from Figs. 1 and 2, respectively.

3-methylbutyloxy (**8c**)] and longer [e.g., octyloxy (**8d**)] substituents gave higher IC_{50} values.

(3) The presence of a ketone group on the quinuclidine skeleton (i.e., compound **9**, Table 1) decreases the activity at both nAChR subtypes. Compare the activity of compound **9** vs **7c** and **8c** (Table 2), which do not have the carbonyl group.

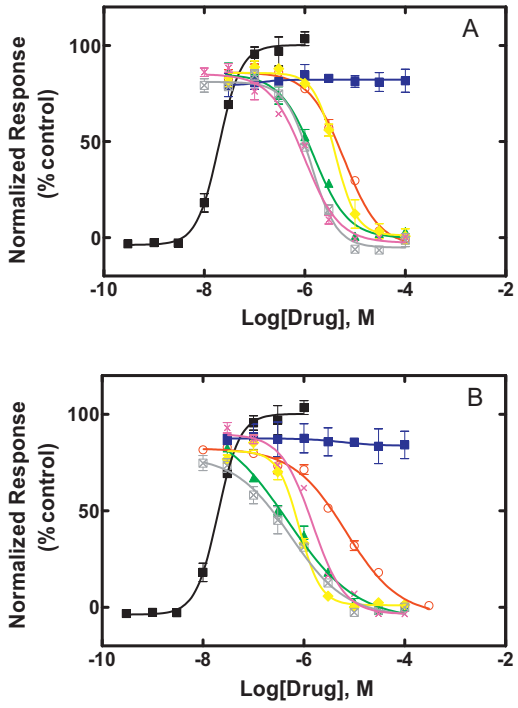

Fig. 1. Inhibitory effect of some compounds shown in Table 1 on (±)-epibatidine-induced Ca^{2+} influx in HEK293-hα4β2 cells. Increased concentrations of (±)-epibatidine (■) activate the hα4β2 nAChR with potency EC_{50} = 1.19 ± 0.08 nM (n = 28). Subsequently, cells were pretreated with several concentrations of: **7a** (■), **7b** (○), **7c** (▲), **7e** (♦), **7i** (☒), **7k** (✕) (see panel A), and **8a** (■), **8b** (○), **8c** (▲), **8e** (♦), **8i** (☒), **8k** (✕) (see panel B), followed by addition of 0.1 μM (±)-epibatidine. The response was normalized to the maximal (±)-epibatidine response which was set to 100%. The plots are representative of three determinations, where the error bars correspond to the standard deviation (SD). The calculated IC_{50} and n_H values are summarized in Table 3.

The fact that the n_H values are close to two for the hα7 nAChR and to one for the hα4β2 nAChR (Table 2) indicates that the inhibitory process is mediated by a cooperative and non-cooperative mechanisms, respectively.

3.3. Radioligand binding results

To establish whether the studied antagonists inhibit the receptors by a competitive or non-competitive mechanism, additional radioligand binding assays were performed. To test the interaction with the orthosteric sites (competitive), the agonist [^{3}H]cytisine was used for the hα4β2 subtype (Fig. 3A) and the selective antagonist [^{3}H]MLA was used for the hα7 subtype (Fig. 4A). To test the interaction with the ion channel (non-competitive), [^{3}H]imipramine was used for both subtypes (Figs. 3B and 4B).

In the case of the hα4β2 nAChR, compounds **7j** and **8j** inhibit [^{3}H]cytisine binding very weakly, with K_i values in the submillimolar-molar concentration range (Table 3). These results indicate that compounds **7j** and **8j** practically do not bind to the orthosteric binding sites but bind with moderate affinities to the [^{3}H]imipramine binding site (Table 3). The observed n_H values are close to unity, indicating that the compounds bind to this site in a non-cooperative manner, and thus suggesting that these compounds bind to just one site. These results support the idea that compounds **7j** and **8j** inhibit the hα4β2 nAChR by a non-competitive mechanism. To determine if the binding affinity of these compounds changes when the receptor is in the resting or desensitizes state, the K_i value for **7j** in the desensitized state (29 ± 4 μM) was compared to that in the resting state (in the presence of 0.1 μM κ-BTx; Arias et al., 2010c). The fact that the calculated K_i value for **7j** in the resting state (19 ± 4 μM; n_H = 1.08 ± 0.20) is in the same concentration range as that in the desensitized state suggests that the compound does not discriminate between these two conformational states. In this regard, no additional experiments were performed in the resting state for the other compounds.

Table 3
Ligand binding affinity for the agonist and ion channel binding sites from the hα7 and hα4β2 nAChRs.

Radioligand	Compound	hα7		hα4β2	
		K_i (μM)	n_H	K_i (μM)	n_H
[^{3}H]MLA	**7i**	10.1 ± 0.9	1.65 ± 0.22	–	–
	7j	14.9 ± 1.4	1.00 ± 0.09	–	–
	8a	2.4 ± 0.2	1.33 ± 0.15	–	–
	8d	1.6 ± 0.1	1.64 ± 0.14	–	–
	8j	5.5 ± 0.3	1.05 ± 0.06	–	–
[^{3}H]Cytisine	**7j**	–	–	>1500	0.55 ± 0.08
	8j	–	–	>470	0.79 ± 0.07
[^{3}H]Imipramine	**7i**	29 ± 5	0.61 ± 0.07	–	–
	7j	30 ± 4	0.55 ± 0.04	29 ± 4	0.82 ± 0.09
	8a	>2700	0.37 ± 0.04	–	–
	8j	104 ± 15	0.78 ± 0.09	75 ± 13	0.92 ± 0.16

The K_i values were calculated from Figs. 3 and 4, according to Eq. (1).

In the case of the hα7 nAChR, the methiodides (**8a**, **8d** and **8j**) and tertiary amines (**7i** and **7j**) bind to the orthosteric ([^{3}H]MLA) sites with higher affinity compared to that for the hα4β2 nAChR (Table 3). Interestingly, the methiodides showed higher affinity than that for the tertiary amines, suggesting that the former derivatives inhibit the hα7 nAChR preferably by a competitive mechanism. Interestingly, the K_i values of compounds **7i** and **7j** (tertiary amines), obtained by [^{3}H]imipramine experiments, are in the same concentration range as those obtained by [^{3}H]MLA experiments, suggesting a dual competitive and non-competitive interaction. However, the n_H values obtained for the [^{3}H]imipramine experiments are close to 0.5, except that for **8j**. These values are in agreement with a negative cooperative interaction, supporting the view that these compounds, except **8j**, inhibit [^{3}H]imipramine binding by an allosteric mechanism. Based on these results, we conclude that the series **7** and **8** derivatives inhibit the hα7 subtype preferably by a competitive mechanism, whereas they inhibit the hα4β2 nAChR preferably by a non-competitive mechanism.

3.4. Molecular docking and molecular dynamics results

Since the compounds were synthesized and tested as racemic mixtures, each enantiomer (*R* or *S*) was docked separately at the hα7 or hα4β2 nAChR. The isomers were docked into each orthosteric site in an independent manner. Each isomer was docked into the orthosteric binding sites to establish the structural features that confer selectivity for either one of these sites. Initial molecular docking results indicate that (*R*)-**8d** interacts preferably with the five orthosteric sites from the hα7 nAChR [see $t = 0$ (cyan) in Fig. 5A]. The same results were obtained for (*S*)-**8d**. Each isomer forms

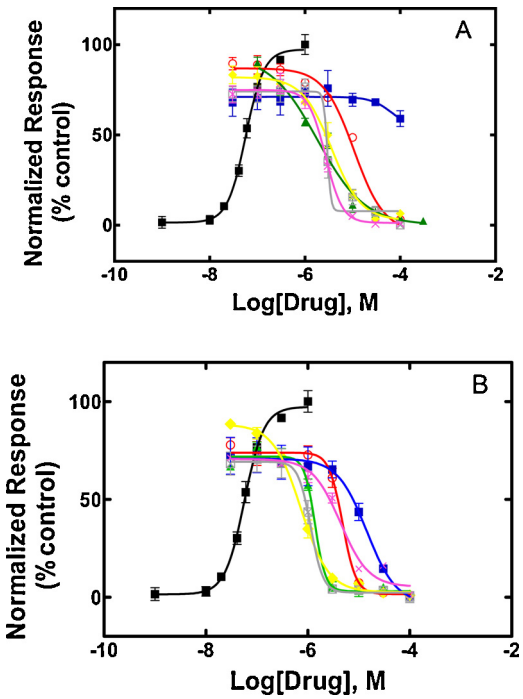

Fig. 2. Inhibitory effect of some compounds shown in Table 1 on (±)-epibatidine-induced Ca^{2+} influx in GH3-hα7 cells. Increased concentrations of (±)-epibatidine (■) activate the hα7 nAChR with potency $EC_{50} = 0.64 \pm 0.23$ nM ($n = 28$). Subsequently, cells were pretreated with several concentrations of: **7a** (■), **7b** (○), **7c** (▲), **7e** (♦), **7i** (☒), **7k** (✕) (see panel A), and **8a** (■), **8b** (○), **8c** (▲), **8e** (♦), **8i** (☒), **8k** (✕) (see panel B), followed by addition of 0.1 μM (±)-epibatidine. The response was normalized to the maximal (±)-epibatidine response which was set to 100%. The plots are representative of three determinations, where the error bars correspond to the standard deviation. The calculated IC_{50} and n_H values are summarized in Table 3.

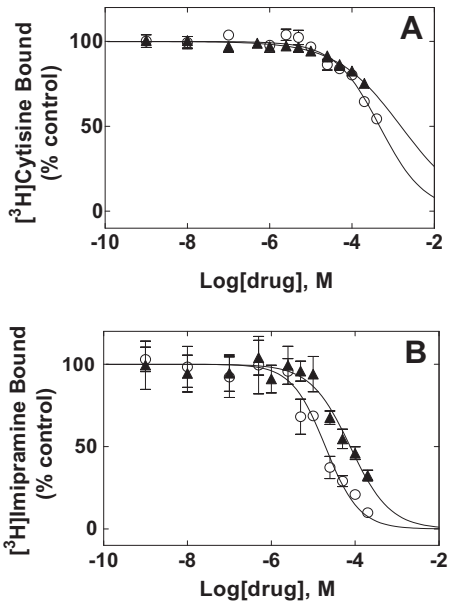

Fig. 3. Ligand interaction with orthosteric and noncompetitive binding sites at the hα4β2 nAChR. Interaction of compounds **7j** (○) and **8j** (▲) with the (A) [^{3}H]cytisine and (B) [^{3}H]imipramine binding sites, respectively. nAChR membranes were preincubated with 7.7 nM [^{3}H]cytisine or 20 nM [^{3}H]imipramine and then equilibrated with increasing concentrations of the ligand under study. Nonspecific binding was assessed at 1 mM CCh or 100 μM imipramine, respectively. Each plot is the combination of separate experiments each performed in triplicate, where the error bars correspond to the standard deviation (SD). The apparent IC_{50} and n_H values were obtained by nonlinear least-squares fit. The K_i values were calculated with Eq. (1) and summarized in Table 4.

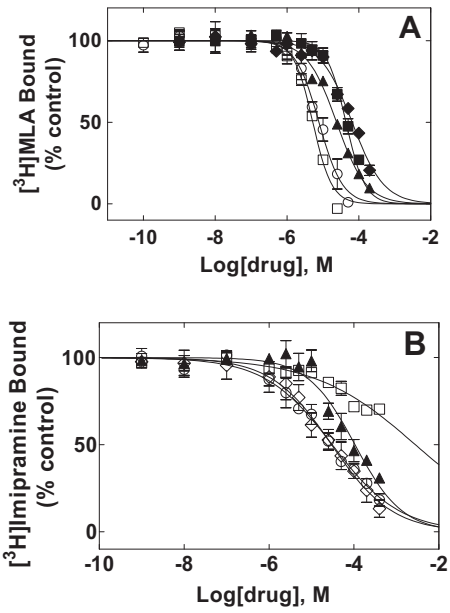

Fig. 4. Ligand interaction with orthosteric and noncompetitive binding sites at the hα7 nAChR. (A) Interaction of compounds **7i** (■), **7j** (♦), **8a** (○), **8d** (□), and **8j** (▲) with the [^{3}H]MLA binding sites. (B) Interaction of compounds **7i** (◊), **7j** (○), **8a** (□), and **8j** (▲) with the [^{3}H]imipramine binding site. nAChR membranes were preincubated with 4.1 nM [^{3}H]MLA or 20 nM [^{3}H]imipramine and then equilibrated with increasing concentrations of the ligand under study. Nonspecific binding was assessed at 1 μM (±)-epibatidine or 100 μM imipramine, respectively. Each plot is the combination of separate experiments each performed in triplicate, where the error bars correspond to the SD. The apparent IC_{50} and n_H values were obtained by nonlinear least-squares fit, according to Eq. (1). The K_i values were calculated with Eq. (1) and summarized in Table 4.

cation-π and van der Waals interactions at the orthosteric sites (Fig. 5C). More specifically, the positively charged nitrogen atom on the quinuclidine moiety from N-methylquinuclidinium derivatives forms cation-π contacts with the aromatic ring from Trp171 at the principal component, whereas the alkoxy moiety (-OR) adopts different conformations in the binding pocket. The lipophilic chain of the ligand also binds by van der Waals interactions to residues from the principal component located within a distance of ~4.5 Å, including Val97, Val132, Val130, Gln139, and Leu141. Although cation-π interactions can be generated for the inactive (i.e., **7a**) and partially (at hα4β2) active (i.e., **8a**) inhibitors, the van der Waals interactions determined for (*R*)-**8d** (Fig. 5C) and its congeners are not observed for **7a** and **8a** (data not shown), suggesting that these interactions are essential for receptor binding. Considering that agonists bind to the principal and complementary components (reviewed in Arias, 2006; Arias et al., 2006; Albuquerque et al., 2009), the lack of interaction with the complementary component may explain why these compounds are not agonists but antagonists.

Considering that cation-π interactions are very important for ligand binding to the hα7 orthosteric sites (Scrutton and Raine, 1996; Arias et al., 2010a), the stability of these interactions was determined by MD experiments (Fig. 5B). The results indicate that the positively charged quaternary ammonium of (*R*)-**8d** becomes closer to the center of the aromatic ring of Trp171 during the 5-ns simulation. The MD results demonstrated that only three of these initial cation-π interactions (i.e., B–D) remained stable (distance < 4 Å) [see *t* = 5 ns (purple) in Fig. 5A]. The insets from Fig. 5A show the difference between the initial and final conformations of (*R*)-**8d** in two orthosteric sites, one stable (i.e., B) and another unstable (i.e., A).

Regarding the docking at the hα4β2 orthosteric sites, (*R*)-**8d** establishes similar interactions but a slightly different orientation respect to that for the hα7 nAChR. This different orientation produces a longer distance (~5.4 Å) between the N from the quinuclidine moiety and the aromatic center of hα4-Trp182 compared to that for hα7-Trp171 (~4.5 Å) (Fig. 5C and D). Therefore, the possibility of forming cation-π interactions at the hα4β2 nAChR is less probable compared to that for the hα7 nAChR, supporting the observed weaker ligand binding affinities for the hα4β2 orthosteric sites (see Table 3).

The docking results at the hα7 and hα4β2 ion channels indicate that the (*S*)-**7j** and (*S*)-**8j** enantiomers bind at luminal binding sites. Similar results were obtained for the (*R*)-**7j** and (*R*)-**8j** enantiomers. Both (*S*)-**7j** and (*S*)-**8j** enantiomers docked within the nAChR ion channels between the serine (hα4β2)/threonine (hα7) (position 6′) and valine (position 13′) rings (Fig. 6A and C). A common feature for both enantiomers is that the best conformers are docked at the same position and in a rather similar way on each nAChR subtype (Fig. 6B and D). However, they seem to have better energy of binding for the hα4β2 ion channel compared to that for the hα7 ion channel (see Table 4). Additional calculations using molecular mechanics methods also support the same conclusion. In this case, the values for the hα4β2 ion channel are −24 [(*S*)-**8j**] and −31 [(*S*)-**7j**] kcal/mol, whereas the values for the hα7 ion channel are −18 and −22 kcal/mol, respectively. The performed 10-ns MD simulations also showed that (*S*)-**7j** and (*S*)-**8j** are more stable in the hα4β2 ion channel compared to that in the hα7 ion channel (Fig. 6E). In both cases, the last 5-ns RMSD values are lower in the hα4β2 ion channel [0.15 and 0.11 Å for (*S*)-**8j** and (*S*)-**7j**, respectively] compared to that for the hα7 ion channel (0.16 and 0.17 Å, respectively). This comparison is statistically significant of the simulations (*t*-Student test; $p < 0.0001$). More importantly perhaps, is the fact that during the last 3-ns of simulation (see thick line in the *x*-axes from Fig. 6E) the movements of (*S*)-**8j** and (*S*)-**7j** in the hα7 ion channel (RMSD variance = 7.7×10^{-6} and 8.5×10^{-6} Å, respectively) are larger than that within the hα4β2 ion channel (2.4×10^{-6} and 1.2×10^{-6} Å, respectively).

4. Discussion

The bicyclic tertiary amine quinuclidine is a well-known moiety that confers selectivity for the α7 nAChR subtype (Mazurov et al., 2006; Horenstein et al., 2008). In this regard, the chemical, functional, and structural characterization of a new series of 2-(substituted benzyl)quinuclidines (**7a**–**k**) and their *N*-methyl-2-(substituted benzyl)quinuclidinium iodides (**8a**–**k**) (see Table 1 for their structures) is studied as possible antagonists of the hα7 and hα4β2 nAChRs.

To determine the inhibitory potency of benzyl quinuclidine derivatives at the hα4β2 and hα7 nAChRs, Ca^{2+} influx experiments were performed in HEK293-hα4β2 (Fig. 1) and GH3-hα7 (Fig. 2) cells. The results indicate that all compounds, except **7a**, are antagonists of the studied nAChRs. The tertiary amines (series **7**) and quaternary ammonium salts (series **8**) showed similar IC_{50}s for the hα4β2 (Table 2). Nevertheless, compounds from series **8**, except **8j** and **8k**, present higher potencies than series **7** at the hα7. These results are in agreement with other quaternary ammonium compounds (Gotti et al., 1998; Simsek et al., 2003; Ragab et al., 2006; Iturriaga-Vásquez et al., 2008; Pérez et al., 2012).

Although the majority of the tested compounds inhibit hα4β2 and hα7 with similar potencies, few exceptions showed some selectivity for one subtype. Compounds **7j** and **8j** showed ~10-fold higher potency at the hα4β2 compared to the hα7, whereas compounds **8b** and **8d** showed ~5-fold higher potency at the hα7 compared to the hα4β2. This suggests that substitutions in the *meta* position (**7j** and **8j**) favor hα4β2 inhibition, whereas *para* substitutions (**8b** and **8d**) favor hα7 inhibition. The observed n_H

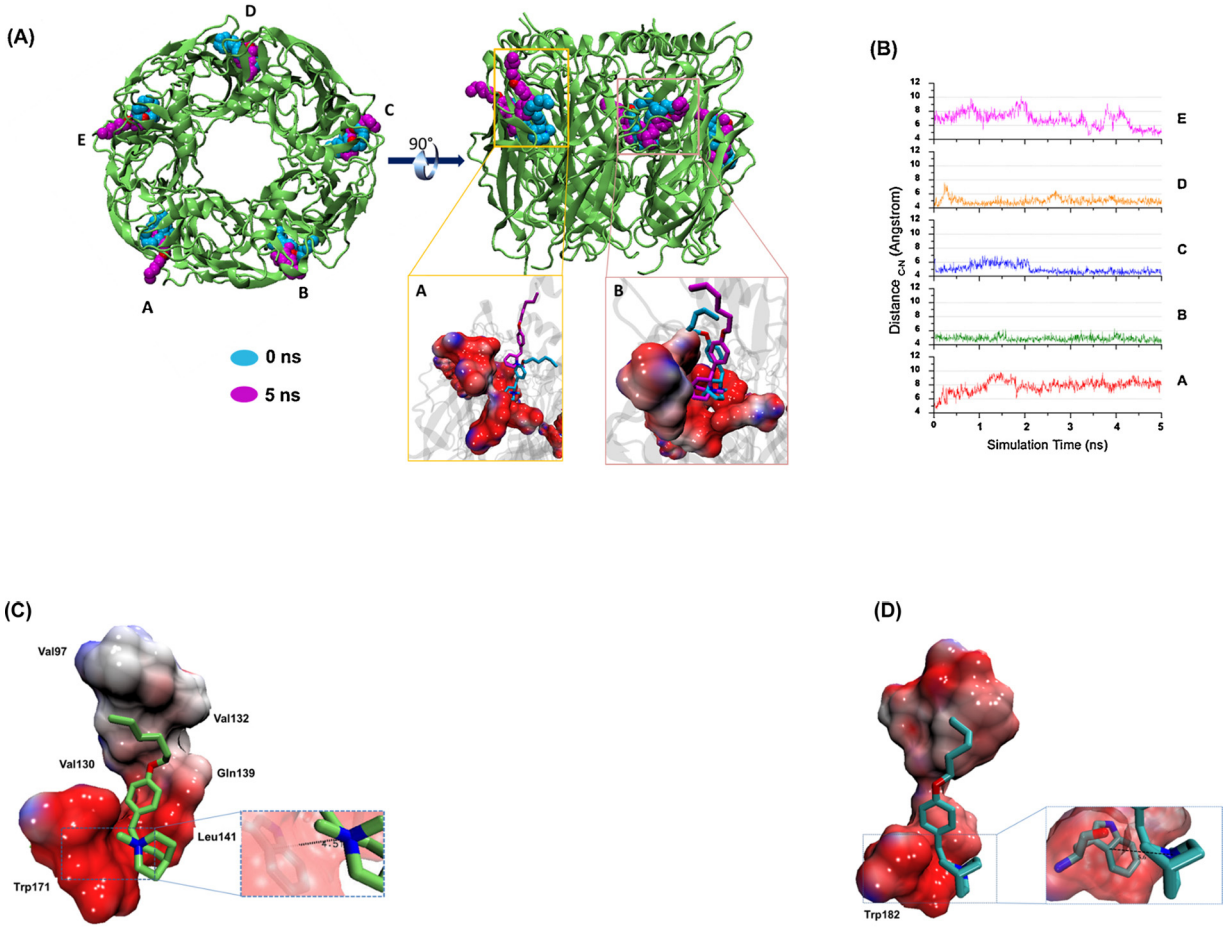

Fig. 5. Molecular interaction of enantiomer (*R*)-**8d** with the hα7 and hα4β2 nAChR orthosteric sites. (A) Extracellular and lateral views of the interaction of (*R*)-**8d** with the five orthosteric sites at the hα7 nAChR determined after molecular docking ($t = 0$, cyan) and after 5 ns of molecular dynamics (MD) simulation ($t = 5$ ns, purple). The insets show the electrostatic potential of the binding cavity and the different molecular orientation of (*R*)-**8d** at sites A (cation-π distance >4 Å; unstable interaction) and B (<4 Å; stable interaction) after 5-ns MD. (B) Each line on the graph represents the MD trajectory of (*R*)-**8d** docked at each one of the five orthosteric sites. The B–D lines correspond to the cation-π interactions that preserve a distance <4 Å during the simulation (i.e., stable interactions), whereas the A and E lines correspond to distances >4 Å (i.e., unstable interactions). (C) Molecular details of the interaction of (*R*)-**8d** with the principal component of one of the hα7 nAChR orthosteric sites. The binding pocket shows the electronic distribution around (*R*)-**8d**. The red color indicates a concentrated electron density (i.e., Trp171 and Leu141), whereas the white color indicates a hydrophobic environment (i.e., Val97, Val130, Val132, and Gln139). The black arrow shows the cation-π interaction between the aromatic ring of Trp171 and the ammonium group from (*R*)-**8d** (distance ~4.5 Å in the inset). In addition, the lipophilic chain of the ligand interacts with non-polar residues by van der Walls contacts. (D) Molecular details of the interaction of (*R*)-**8d** with the principal component of one of the hα4β2 nAChR orthosteric sites. Although the general aspects of the ligand interaction is similar to that for the hα7 nAChR, the distance between the ligand's ammonium group and the aromatic ring of Trp182 (analogous to hα7-Trp171) is longer (~5.6 Å; see black arrow) compared to that for the hα7 nAChR. (For interpretation of the references to color in this figure legend, the reader is referred to the web version of this article.)

values suggest that the compounds bind to only one (hα4β2) or to two or more sites (hα7), respectively. Such result is not surprising because the α7 nAChR has five agonist sites and at least three of them must be occupied to active it (Rayes et al., 2009). In fact, our docking and MD results indicate that the interaction of compound (*R*)-**8d** with the hα7 nAChR binding sites is stable for three of them (i.e., sites B–D in Fig. 5A).

The radioligand competition results indicate that the compounds interact with the hα7, but not hα4β2, orthosteric sites (Table 3). In the hα7, the methiodides **8a**, **8d** and **8j** bind with higher affinities than that for **7i** and **7j**. These results coincide with the higher inhibitory potency of the quaternary salts at the hα7 compared to that at the hα4β2 (Table 2). Interestingly, the [^{3}H]imipramine competition results indicate that compounds **7j** and **8j** inhibit the hα4β2 by binding preferably to the ion channel compared to the agonist sites (52- and 6-fold difference). The opposite is true for the hα7, where **8a** and **8j** bind the agonist sites with 1125- and 19-fold higher affinity than that for the ion

Table 4
Ligand binding energy for different sites at the hα7 and hα4β2 nAChRs.

Compound	Binding site	nAChR subtype	Emulated binding energy (kcal/mol)	Binding energy ratio hα4β2/hα7
(*R*)-**8d**	Orthosteric	hα4β2	−9.0	
		hα7	−9.5	0.95
(*S*)-**8j**	Luminal	hα4β2	−8.8	
		hα7	−7.8	1.13
(*S*)-**7j**	Luminal	hα4β2	−8.4	
		hα7	−7.7	1.09

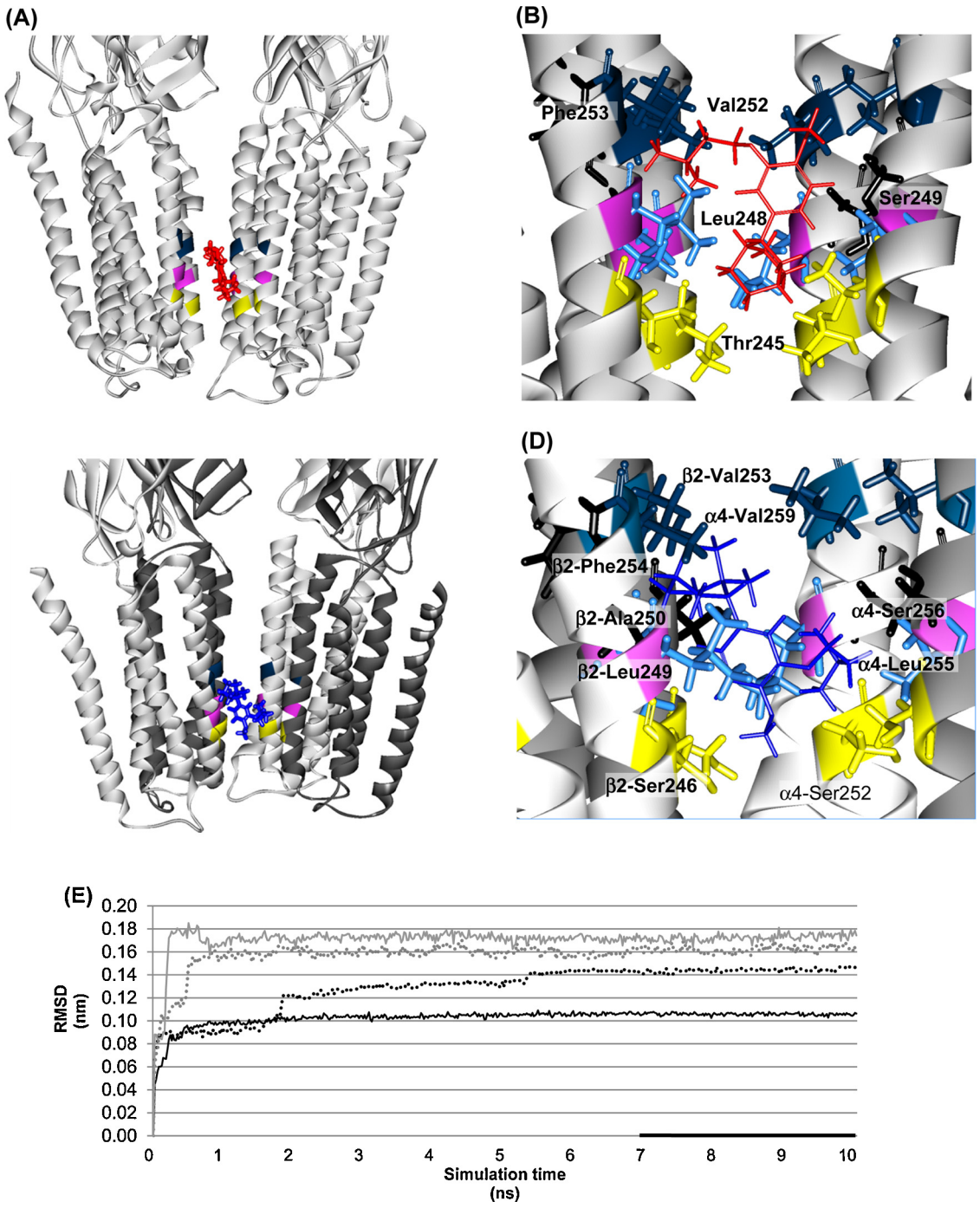

Fig. 6. Molecular interactions of enantiomers (*S*)-**7j** (red) and (*S*)-**8j** (blue) within the hα7 and hα4β2 nAChR ion channels. The (*R*)-enantiomers present the same locations. The threonine (hα7)/serine (hα4β2) (position 6′), leucine (position 9′), and valine (position 13′) rings are in yellow, purple, and violet, respectively. For the hα4β2 nAChR, the α4 subunits are represented in dark gray. One of the subunits (i.e., β2 for the hα4β2 nAChR) was hidden for clearness. (A) Binding site location for (*S*)-**7j** (red) within the hα7 nAChR ion channel. The binding site location for (*S*)-**8j** is similar. (B) Molecular details of the interaction of (*S*)-**7j** within the hα7 nAChR ion channel. In addition to the residues from rings 6′ (Thr245), 9′ (Leu248), and 13′ (Val252), other residues (in black) make contact with this conformer, including Phe253 (position 14′) and Ser249 (position 10′) from one α7 subunit as well as two more Ser249 residues from non-adjacent subunits. All interactions are hydrophobic, and no hydrogen bond or cation-π interactions were detected. (C) Binding site location for (*S*)-**8j** (blue) within the hα4β2 nAChR ion channel. The binding site location for (*S*)-**7j** is similar. (D) Molecular details of the interaction of (*S*)-**8j** within the hα4β2 nAChR ion channel. In addition to the residues from rings 6′ (α4-Ser252 and β2-Ser246), 9′ (α4-Leu255 and β2-Leu249), and 13′ (α4-Val259 and β2-Val253), other amino acids (in black) make contact with this conformer, including two α4-Ser256 and two β2-Ala250 residues (position 10′) from non-adjacent subunits, and β2-Phe254 (position 14′) from an adjacent β2 subunit. All interactions are hydrophobic in nature. (E) Molecular dynamics simulations of (*S*)-**7j** (—) and (*S*)-**8j** (. . .) docked within the hα7 (gray) and hα4β2 (black) nAChR ion channels, respectively. RMSD is the root mean square deviation from the initial docking position (see Supplemental Information for more details). The thick line in the *x*-axis shows the time span of the measured RMSD variance for (*S*)-**7j** (7.7×10^{-6} Å) and (*S*)-**8j** (8.5×10^{-6} Å) at the hα7 nAChR, and for the same ligands (2.4×10^{-6} and 1.2 10^{-6} Å, respectively) at the hα4β2 nAChR. (For interpretation of the references to color in this figure legend, the reader is referred to the web version of this article.)

channel. These results are supported by the docking and MD studies, where the energies of binding of (*S*)-**7j** and (*S*)-**8j** with the hα4β2 ion channel show a favorable trend (Table 4) and are more stable compared with the hα7 channel (Fig. 6).

Collectively, our results indicate that the *para* substituted methiodide salt derivatives (i.e., **8b**, **8d**, and **8g**) are the best competitive antagonists for the hα7, whereas the *meta* substituted methiodides and hydrochloride salt derivatives (i.e., **7b**–**7k**) are comparatively weaker hα7 antagonists. Both series of compounds inhibit the hα4β2 mainly by a non-competitive mechanism, by overlapping the luminal imipramine site located in the middle of the ion channel.

Acknowledgements

This research was supported by grants from Fondo Nacional de Desarrollo Científico y Tecnológico (FONDECYT, Chile) (#11090120) and Millennium Scientific Initiative (Ministerio de Economía, Fomento y Turismo, Chile) (Grant P10-035-F) (to E.G.P.), and from the Consejo Nacional de Investigaciones Científicas y Técnicas (CONICET, Argentina) (to M.O.O.).

Appendix A. Supplementary data

Supplementary data associated with this article can be found, in the online version, at http://dx.doi.org/10.1016/j.biocel.2013.08.003.

References

Albuquerque EX, Pereira EFR, Alkondon A, Rogers SW. Mammalian nicotinic acetylcholine receptors: from structure to function. Physiological Reviews 2009;89:73–120.

Ángyán JG. Choosing between alternative MP2 algorithms in the self-consistent reaction field theory of solvent effects. Chemical Physics Letters 1995;241:51–6.

Arias HR. Ligand-gated ion channel receptor superfamilies. In: Arias HR, editor. Biological and biophysical aspects of ligand-gated ion channel receptor superfamilies. Kerala, India: Research Signpost; 2006. p. 1–25.

Arias HR, Bhumireddy P, Bouzat C. Molecular mechanisms and binding site locations for noncompetitive antagonists of nicotinic acetylcholine receptors. International Journal of Biochemistry and Cell Biology 2006;38:1254–76.

Arias HR, Gu H, Feuerbach D, Wei D-Q. Different interaction between the agonist JN403 and the competitive antagonist methyllycaconitine with the human α7 nicotinic receptor. Biochemistry 2010a;49:4169–80.

Arias HR, Feuerbach D, Targowska-Duda KM, Russell MM, Jozwiak K. Interaction of serotonin selective reuptake inhibitors with neuronal nicotinic acetylcholine receptors. Biochemistry 2010b;49:5734–42.

Arias HR, Rosenberg A, Targowska-Duda KM, Feuerbach D, Jozwiak K, Moaddel R, et al. Tricyclic antidepressants and mecamylamine bind to different sites in the human α4β2 nicotinic receptor ion channel. International Journal of Biochemistry and Cell Biology 2010c;42:1007–18.

Arias HR, Gu R-X, Feuerbach D, Gu B-B, Ye Y, Wei D-Q. Novel positive allosteric modulators of the human α7 nicotinic receptor. Biochemistry 2011;50:5263–78.

Blum AP, Lester HA, Dougherty DA. Nicotinic pharmacophore: the pyridine N of nicotine and carbonyl of acetylcholine hydrogen bond across a subunit interface to a backbone NH. Proceedings of the National Academy of Sciences of the United States of America 2010;107:13206–11.

Celie PHN, Van Rossum-Fikkert SE, Van Dijk WJ, Brejc K, Smit AB, Sixma TK. Nicotine and carbamylcholine binding to nicotinic acetylcholine receptors as studied in AChBP crystal structures. Neuron 2004;41:907–14.

Cheng Y-C, Prusoff WH. Relationship between the inhibition constant (Ki) and the concentration of inhibitor which causes 50 per cent inhibiton IC50 of an enzymatic reaction. Biochemical Pharmacology 1973;22:3099–108.

Chipot C, Maigret B, Rivail J-L, Sheraga HA. Modeling amino-acid side-chains. 1. Determination of net atomic charges from abinitio self-consistent-field molecular electrostatic properties. Journal of Physical Chemistry 1992;96:10276–84.

Corpet F. Multiple sequence alignment with hierarchical clustering. Nucleic Acids Research 1988;16:10881–90.

Crooks PA, Ravard A, Wilkins LH, Teng LH, Buxton ST, Dwoskin LP. Inhibition of nicotine-evoked [^{3}H]dopamine release by pyridino *N*-substituted nicotine analogs – a new class of nicotinic antagonist. Drug Development Research 1995;36:91–102.

Davies AR, Hardick DJ, Blagbrough IS, Potter BV, Wolstenholme AJ, Wonnacott S. Characterisation of the binding of [^{3}H]methyllycaconitine: A new radioligand for labelling α7-type neuronal nicotinic acetylcholine receptors. Neuropharmacology 1999;38:679–90.

Ferchmin PA, Pérez D, Castro Álvarez W, Penzo MA, Maldonado HM, Eterovic VA. γ-Aminobutyric acid type a receptor inhibition triggers a nicotinic neuroprotective mechanism. Journal of Neuroscience Research 2013., http://dx.doi.org/10.1002/jnr.23155.

Feuerbach D, Nozulak J, Lingenhoehl K, McAllister K, Hoyer D. JN403, *in vitro* characterization of a novel nicotinic acetylcholine receptor α7 selective agonist. Neuroscience Letters 2007;416:61–5.

Frisch MJ, Trucks GW, Schlegel HB, Scuseria, GE, Robb MA, Cheeseman JR, et al. Gaussian, Inc., Wallingford, CT; 2004.

Gotti C, Balestra B, Moretti M, Rovati GE, Maggi L, Rossoni G, et al. 4-Oxystilbene compounds are selective ligands for neuronal nicotinic α-bungarotoxin receptors. British Journal of Pharmacology 1998;124:1197–206.

Grubmueller H. SOLVATE v. 1.0. Theoretical Biophysics Group, Institute for Medical Optics, Ludwig-Maximilians University, Munich; 1996.

Horenstein NA, Leonik FM, Papke RL. Multiple pharmacophores for the selective activation of nicotinic α7-type acetylcholine receptors. Molecular Pharmacology 2008;74:1496–511.

Humphrey W, Dalke A, Schulten K. VMD: visual molecular dynamics. Journal of Molecular Graphics 1996;14:33–8.

Hurst R, Rollema H, Bertrand D. Nicotinic acetylcholine receptors: from basic science to therapeutics. Pharmacology & Therapeutics 2013;137:22–54.

Iturriaga-Vásquez P, Pérez EG, Slater EY, Bermúdez I, Cassels BK. Aporphine metho salts as neuronal nicotinic acetylcholine receptor blockers. Bioorganic and Medicinal Chemistry 2008;15:3368–72.

Mazurov A, Hauser T, Selective Miller CH. α7 nicotinic acetylcholine receptor ligands. Current Medicinal Chemistry 2006;13:1567–84.

Morris GM, Goodsell DS, Halliday RS, Huey R, Hart WE, Belew RK, et al. Automated docking using a Lamarckian genetic algorithm and an empirical binding free energy function. Journal of Computational Chemistry 1998;19:1639–62.

Mousa SA, Arias HR. Angiogenesis modulation by nicotine and nicotinic ligands. Journal of Pediatric Biochemistry 2010;1:91–104.

Paleari L, Cesario A, Fini M, Russo P. α7-Nicotinic receptor antagonists at the beginning of a clinical era for NSCLC and mesothelioma. Drug Discovery Today 2009;14:822–36.

Pérez EG, Cassels BK, Eibl C, Gündisch D. Synthesis and evaluation of N1-alkylindole-3-ylalkylammonium compounds as nicotinic acetylcholine receptor ligands. Bioorganic and Medicinal Chemistry 2012;20:3719–27.

Pérez EG, Ocampo C, Feuerbach D, López JJ, Morelo GL, Tapia RA, et al. Novel 1-(1-benzyl-1H-indol-3-yl)-NNN-trimethylmethanaminium iodides are competitive antagonists of the human α4β2 and α7 nicotinic acetylcholine receptors. Medicinal Chemistry Communications 2013;4:1166–70, http://dx.doi.org/10.1039/C3MD00042G.

Phillips JC, Braun R, Wang W, Gumbart J, Tajkhorshid E, Villa E, et al. Scalable molecular dynamics with NAMD. Journal of Computational Chemistry 2005;26:1781–802.

Ragab HM, Kim JS, Dukat M, Navarro H, Glennon RA. Aryloxyethylamines: binding at α7 nicotinic acetylcholine receptors. Bioorganic and Medicinal Chemistry Letters 2006;16:4283–6.

Rayes D, De Rosa MJ, Sine SM, Bouzat C. Number and locations of agonist binding sites required to activate homomeric Cys-loop receptors. Journal of Neuroscience 2009;29:6022–32.

Romanelli MN, Gratteri P, Guandalini L, Martini E, Bonaccini C, Gualtieri F. Central nicotinic receptors: Structure, function, ligands, and therapeutic potential. ChemMedChem 2007;2:746–67.

Sadek B, Ashoor A, Mansouri AA, Lorke DE, Nurulain SM, Petroianu G, et al. N3,N7-Diaminophenothiazinium derivatives as antagonists of α7-nicotinic acetylcholine receptors expressed in *Xenopus* oocytes. Pharmacological Research 2012;66:213–8.

Šali A, Blundell TL. Comparative protein modelling by satisfaction of spatial restraints. Journal of Molecular Biology 1993;234:779–815.

Scheiber P, Nemes P. Short synthesis of 2,3,4,5-tetrahydrocytisine. ARKIVOC 2008;iii:194–9.

Scrutton NS, Raine ARC. Cation-π bonding and amino–aromatic interactions in the biomolecular recognition of substituted ammonium ligands. Biochemical Journal 1996;319:1–8.

Sheridan RD, Smith AP, Turner SR, Tattersall JE. Nicotinic antagonists in the treatment of nerve agent intoxication. Journal of the Royal Society of Medicine 2005;98:114–5.

Simsek R, Chang-Fong J, Lee M, Dukat M, Damaj MI, Martin BR, et al. Quaternary ammonium 3-(aminoethoxy)pyridines as antinociceptive agents. Bioorganic and Medicinal Chemistry Letters 2003;13:2917–20.

Strachan JP, Farias JJ, Zhang J, Caldwell WS, Bhatti BS. Diazaspirocyclic compounds as selective ligands for the α4β2 nicotinic acetylcholine receptor. Bioorganic and Medicinal Chemistry Letters 2012;22:5089–92.

Trott O, Olson AJ. AutoDock Vina: improving the speed and accuracy of docking with a new scoring function, efficient optimization and multithreading. Journal of Computational Chemistry 2010;31:455–61.

Tuppo EE, Arias HR. The role of inflammation in Alzheimer's disease. International Journal of Biochemistry and Cell Biology 2005;37:289–305.

Unwin N. Refined structure of the nicotinic acetylcholine receptor at 4 Å resolution. Journal of Molecular Biology 2005;346:967–89.
Vijayakumar N, Sean P, Peter A. (Z)-2-(3-Hydroxy-4-methoxybenzyl-idene)-1-azabicyclo[2.2.2]octan-3-one. Acta Crystallographica Section C: Crystal Structure Communications 2003;C59:o647–9.
Vijayakumar N, Sean P, Peter A. (Z)-2-(3-Methoxybenzylidene)-1-aza-bicyclo[2.2.2]octan-3-one. Acta Crystallographica Section C: Crystal Structure Communications 2005;61:o660–1.
Zhang J, Steinbach JH. Cytisine binds with similar affinity to nicotinic α4β2 receptors on the cell surface and in homogenates. Brain Research 2003;959:98–102.